J Mater Sci: Mater Med (2011) 22:1365–1374
DOI 10.1007/s10856-011-4318-3

Elasticity, thermal stability and bioactivity of polyhedral oligomeric silsesquioxanes reinforced chitosan-based microfibres

S. L. Chew · K. Wang · S. P. Chai · K. L. Goh

Received: 21 January 2011 / Accepted: 6 April 2011 / Published online: 20 April 2011

Abstract A wet-spinning approach was used to extrude ribbon-like micrometer-thick fibres comprising chitosan with 1, 3, 5, 7 and 9% (w/w) polyhedral oligomeric silsesquioxanes (POSS). ANOVA reveals significant variations in the maximum stress (σ), stiffness (E), elastic energy storage (u') and fracture toughness (u) of the microfibres with respect to POSS concentration: σ, u' and u peak at 7% (w/w) but POSS concentration has no effect on E. Scanning electron microscopy of the ruptured microfibres reveals fracture and detachment of POSS precipitates from the chitosan matrix. Bioactivity test using simulated body fluids reveals a net gain in mass (by day 4) and grossly distorted morphology caused by apatite deposition on the microfibre surface. Fourier transform infrared spectroscopy reveals that chitin is partially deacetylated into chitosan and it further shows the presence of POSS in the microfibres. Thermogravimetric analysis shows that the microfibres are thermally stable up to 240°C in a nitrogen atmosphere.

1 Introduction

This report presents a study on the synthesis, characterisation and analysis of the underlying structure–property relationship of bioactive and thermally stable chitosan-based microfibres reinforced by polyhedral oligomeric silsesquioxanes (POSS) particulates. Increasingly, naturally occurring materials such as chitosan, being native to the local environment, have been used to fabricate microfibres with properties mimicking those of extracellular matrix of connective tissues [1–5]. From structural point of view, these are suitable for tissue engineering applications such as tissue repair or regeneration [6]. In particular, these microfibres can be assembled to form a scaffold with enhanced surface to volume ratio (compared to a monolithic material) for cell attachment and proliferation into the microstructure [7–9]. Chitosan is a deacetylated linear polysaccharide found in high abundance in the exoskeleton of crustacean (e.g. shrimps). From tissue engineering point of view, chitosan is useful owing to its ability to clot blood rapidly, promote healing and produce hypoallergenic response, biocompatibility, bio-degradability and nontoxicity [10–12]. For manufacturing purposes, chitosan is easily molded into a wide variety of shapes, such as beads, filaments and membranes [10].

Of major concern in the engineering of biomaterials as scaffolds for connective tissues is the mechanical compatibility with the host tissue [13]. Here, the aim is to minimize regions of mismatch in mechanical properties that could otherwise induce high stress concentration when the repaired tissue is loaded. The tensile strength and modulus of elasticity of chitosan membrane ranges 3–10 MPa and 4–8 MPa, respectively (depending on the degree of branching, i.e. ranging 1.6–80 kDa [14]). It is important to note that on order of magnitude comparison the strength and stiffness of chitosan is mechanically compatible with cartilage; the latter is characterized by a maximum stress of 0.5–2.5 MPa [15, 16] and a compressive stiffness of 0.45–0.80 MPa [17], depending on the age

S. L. Chew
School of Chemical and Biomedical Engineering, Nanyang Technological University, Singapore 637457, Singapore

K. Wang
Department of Chemical Engineering, The Petroleum Institute, Abu Dhabi, United Arab Emirates

S. P. Chai · K. L. Goh (✉)
School of Engineering, Monash University Sunway Campus, Selangor 46150, Malaysia
e-mail: goh.kheng.lim@eng.monash.edu.my

of the individual and the anatomical location of the tissue. However, this is not the case with bone which exhibits a flexural modulus of elasticity of 10–18 GPa and a flexural strength of 120–180 MPa [18, 19]. One approach to overcome the mechanical incompatibility is to reinforced chitosan by an inorganic compound. POSS are cage-like hybrid inorganic–organic molecules (1–3 nm in size) with chemical composition of silicon and oxygen (of the form Si_8O_{12}) which can accommodate various functional groups by binding each group to the respective Si atom [20, 21]. The POSS nanostructures are resorbable, bioactive and biocompatible; in vitro immuno-histochemistry experiments have shown that POSS encourages the proliferation and differentiation of bone stroma cell and the deposition of apatite [22]. POSS and chitosan do not exist together as blends in nature, but the specific properties of each may be used to produce blends that yield unique structural and mechanical properties.

Here, for the first time, we report the synthesis of ribbon-like POSS-chitosan (PC) microfibres based on a similar approach implemented for an earlier study for hydroxyapatite-chitosan microfibres [3]. The preparation of composite polymer with the desirable properties is influenced by many variables including the type of reinforcement particle, solvent, component ratio, temperature, pressure, pH and preparation conditions [23]. In this study the sensitivity of the mechanical properties of the microfibres was investigated by varying the POSS concentration. Tensile test was carried out to determine the tensile strength (σ), stiffness (E), elastic storage energy (u') and fracture toughness (u) of the microfibres. Surface morphology was examined by scanning electron microscopy (SEM). Compositional study was carried out using Fourier Transform Infra-red (FT-IR) spectroscopy. Thermal stability was evaluated by thermogravimetric analysis (TGA). Biodegradation of the microfibres was investigated by immersing the microfibres in a simulated body fluid (SBF) environment.

2 Materials and methods

2.1 Synthesis

Schematic of the PC microfibre synthesis process is shown in Fig. 1. De-ionized (DI) water (Milli-Q unit, Millipore, USA) was used to prepare all the solutions/suspensions in this study. A solution containing 1.5 w/v% (1 w/v% is equivalent to 0.01 g/ml) of chitosan to acetic acid was prepared by dissolving 0.15 g of flake purified chitosan (approximately 100 kDa, 85% deacetylated, from Sigma-Aldrich, USA) in 10 ml of 1 wt% acetic acid (the acetic acid solution was obtained by diluting reagent grade glacial acetic from Sigma-Aldrich, USA). The mixture was stirred

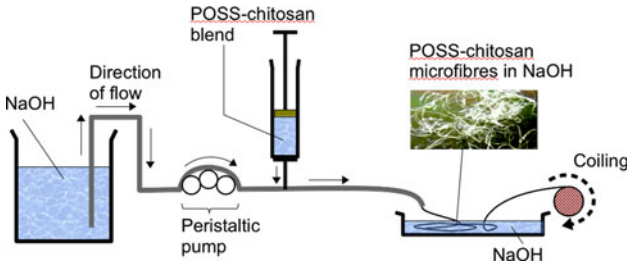

Fig. 1 Schematic of the POSS-chitosan microfibre synthesis process

at 700 rpm at room temperature for 4 h to dissolve the chitosan completely. Any loss of solution by evaporation was minimized by covering the container with a tight aluminum foil. Following this, the solution was divided into six portions. The first portion was designated as control. The inorganic phase used for blending into the chitosan solution was aminopropylphenyl POSS (AM0272, Hybrid Plastic Inc. USA), which is a white powder. The molecular formula for aminopropylphenyl POSS is $C_{45}H_{43}NO_{12}Si_8$, comprising two functional groups, aminopropyl ($NH_2CH_2CH_2CH_2$) [24], phenyl (C_6H_5) [25], and the core cage-like molecule (Si_8O_{12}) [26]. Thus, to the remaining five portions, predetermined amounts of the POSS compound at 1, 3, 5, 7 and 9% (w/w), corresponding to 0.0015 g, 0.0045 g, 0.0075 g, 0.0105 g and 0.0135 g, respectively, were added and the resultant mixtures were stirred at 700 rpm at room temperature for 18 h to completely dissolve the POSS.

A predrawn wet spun fiber extrusion approach [3, 27] was implemented in this study to fabricate the microfibres. Each of the six portions of PC blend was channeled through a blunt-end needle (27G) at a rate of 3 cm/min (single syringe pump, NE1000, BioLynx, Quebec, Canada) from a 10 ml syringe (BD Medical, New Jersey, US) into a stream of coagulant solution containing 1 M of NaOH (Sigma-Aldrich, USA), at a junction 22 cm away from the exit. Thus, POSS precipitated to form crystallites within the microfibre inside the tube before they were extruded through a 1.6 mm (inner) diameter epoxy-cured silicone tube at a rate of 1 ml/min using a peristaltic pump, together with the coagulant solution. During this stage, the POSS aggregates form raft-like and sheet-like particulates within the chitosan matrix [28, 29]. The flow action during extrusion facilitated the alignment of these particulates in the direction of the axis of the PC microfibre so that the particulates would be able to provide axial reinforcement to the fibre. At the exit, the microfibres were collected into another coagulant solution (1 M NaOH) and left in the solution for 15 min; thereafter they were removed from the coagulant solution for rinsing with DI water, followed by soaking in methanol (for 15 min) to remove moisture. Finally, the microfibres were removed from the methanol

bath by winding over a 5-cm glass cylinder for air-drying at room temperature [30]. Winding the microfibres around a cylinder was also intended to constrain the microfibre by lateral deformation to achieve a ribbon-like cross section.

2.2 Electron microscopy

The morphology of the microfibres was examined using a high-resolution JEOL JSM-6390LA field-emission SEM (FESEM). Images of the following regions on the microfibres were acquired: (1) the severed ends (prepared using a surgical blade), (2) the fractured ends (i.e. from mechanical testing; see Sect. 2.6) and (3) surfaces of the microfibre (modified by the simulated body fluid; see Sect. 2.5).

2.3 Fourier transform infrared spectroscopy

FT-IR spectroscopic analysis of the compositional characteristics of the functional groups of the microfibres was carried out using FTS3100 (Varian Inc., USA). Approximately 2 mg of each sample was embedded in 100 mg KBr and the mixture was pressed into discs. The FT-IR sample compartment was continuously purged with dry air to prevent the formation of water vapor. All spectra were obtained from 400 to 4000 cm^{-1} with 36 scans per specimen, at 4 cm^{-1} resolution, and averaged to obtain a representative plot. Background subtraction was carried out by software.

2.4 Thermogravimetric analysis

The degradation temperature of the microfibres was determined by thermogravimetric analysis (TGA) (SDT Q600 V8.0, Build 95, USA) which was carried out in nitrogen atmosphere from ambient temperature to 500°C with a heating rate of 10°C/min. The samples were placed in a platinum pan and purified nitrogen purge of 100.0 ml/min was introduced into the TGA.

2.5 Simulated body fluids

In order to model the condition in human blood plasma for investigating the rate of degradation of the microfibre in the human body, 50 mg of each microfibre was prepared before immersing in a SBF (pH 7.4) containing ion concentrations similar to that of human blood plasma. Here, the SBF was prepared by dissolving the following reagents in DI water: 0.412 g of NaCl (141 mM), 0.0149 g of KCl (4.0 mM), 0.0030 g of $MgSO_4{\cdot}6H_2O$ (0.5 mM), 0.0102 g of $MgCl_2$ (1.0 mM), 0.0176 g of $NaHCO_3$ (4.2 mM), 0.0184 g of $CaCl_2{\cdot}2H_2O$ (2.5 mM), and 0.0680 g of K_2HPO_4 (1.0 mM) [31, 32]. All reagents were obtained from Sigma–Aldrich, USA. During the experiment, the simulated body fluid was buffered using tris(-hydroxymethyl)-aminomethane ($(CH_2OH)_3CNH_2$) and hydrochloric acid (HCl), at a temperature of 36.5°C, for a maximum of 4 days. At the end of the experiment, the microfibres were washed with DI water, dried at room temperature, and weighed.

2.6 Mechanical testing

A high-throughput small-scale horizontal tensile test rig (developed in-house) was used to determine the tensile properties of the microfibres. For a detailed description of the rig see Goh et al. [33, 34]. The microfibres were severed to yield several samples with length of 8 cm. For each group, fifteen samples were randomly selected. Each sample was mounted onto a paper template using a cyanoacrylate adhesive; grip plates were used to secure the specimen-template on the rig. The sample was stretched to rupture at a displacement rate of 0.06 mm/s to model normal physiological loading [3, 33, 34].

Force (F) and grip-to-grip displacement (Δ) were recorded for each specimen; they were used to derive the corresponding nominal stress ($=F/\alpha$) and strain ($=\Delta/l_o$) (Fig. 2). Here, α is the cross-section area of each specimen; l_o is the gauge length of the microfibre which corresponds to the initial grip-to-grip distance (adjusted until just before the specimen became taut). Linear regression analysis was carried out to fit a curve (a third order polynomial equation) to the points from the origin of the stress–strain plot to (σ, ε); here ε represents the strain corresponding to σ. From this curve, we determined the point of inflexion; the gradient at this point is used to parameterize the stiffness of the microfibre, E [33, 34]. In addition, we have sought to determine the following areas under the curve: (1) from the origin to the point of inflexion to parameterize the elastic stored energy until yielding occurs, u', and (2) from the origin to (σ, ε) to parameterize the fracture toughness of the microfibre, u [34]. Thus u' is intended to describe the energy stored in the bonds within the POSS precipitate, leading to elastic deformation of the microfibre which, upon removal of the load, will be released as the microfibre undergoes relaxation. We note that the true elastic energy could extend beyond the point of inflexion so that the magnitude of u' determined by this method may be underestimated. On the other hand, u is intended to describe the stored energy required for creating new crack surfaces.

The stage of an inverted light microscope (TS100, Nikon) was used for accommodating the rig for monitoring the microfibre during tensile loading. The microscope was also used for quantifying α. Here, we note that the microfibre has ribbon-like shape (Fig. 3a) with a near-triangular cross section. The thickness (t) and width (w) of cross sections at five different locations were recorded to

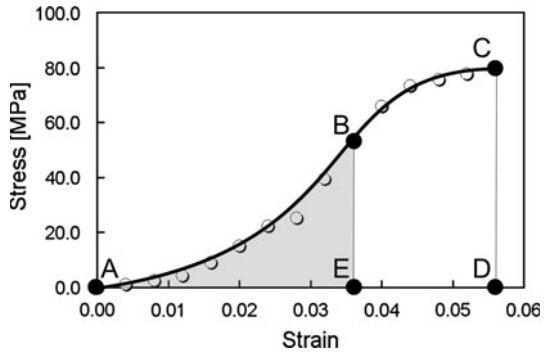

Fig. 2 Determining the stress–strain parameters for a POSS-chitosan microfibre. Using linear regression analysis, a third-order polynomial equation, described by a non-linear line (*ABC*), was fitted to the data points from the origin until maximum stress (σ) at point *C*, which represents the strength of the microfibre. The gradient at the point of inflexion (*B*) is used to describe the stiffness of the microfibre. The shaded area corresponds to the elastic strain energy density (u'). The total strain energy density to fracture (u) corresponds to the area under the fitted line from *A* to *C*

calculate α (=[1/2]tw); the average of α was designated as the representative value of the test sample.

2.7 Statistical analysis

As the deviations of the data from the regression line (residuals) follow a normal distribution have uniform variance, one-way ANOVA, together with Tukey's comparison of the mean values (family error rate = 0.01), was used to analyze for sensitivity of the respective mechanical parameter to POSS concentration. Differences due to the treatment were considered significant if the *P*-value $<$ 0.01. To test for evidence of a relationship, namely σ versus POSS concentration, linear regression analysis, otherwise known as Pearson's correlation, was used. The test statistics F-ratio (ANOVA) was evaluated at a level of significance = 0.01. For informational purposes, representative values (mean $\pm$ standard error) of the mechanical parameters, namely σ, E, u' and u, were determined for each POSS concentration and plotted using bar charts.

3 Results

3.1 Microscopic appearances

All microfibres reveal a bulging axis which tapers off towards the edges (Fig. 3a); consequently they appear translucent near the edge but become increasingly opaque towards the fibre axis (Fig. 3a). All microfibres reveal no appreciable deformation (such as necking) at the fractured ends (Fig. 3a); the edge and surface of these ends are near perpendicular to the axis of the microfibre. All these suggest that the microfibres fail by brittle fracture. At high magnification, SEM images of the fractured ends reveal numerous fissures and projections across the cross section (Fig. 3b); these may be attributed to the detachment of POSS crystallites from the chitosan matrix (intergranular failure) or fracture of POSS crystallites (transgranular failure). Figure 3c shows the morphology of the ends of microfibres that was severed using a blade; in this case, the cross section features a relatively smoother texture, albeit a few ridges which are attributed to scratches caused by the blade.

3.2 Mechanical properties

The stress–strain response for all microfibres exhibits a non-linear relationship from initial loading until fracture (Fig. 2). The mechanical response is characterized by a gradual non-linear increase in the stress as the stress increases from zero until the point of inflexion. Correspondingly the gradient is small at initial loading and increases until it reaches a maximum at the point of inflexion. Thereafter the gradient decreases to a minimum value as the stress increases to σ. Beyond σ the microfibre fractures catastrophically as is portrayed by the rapid decrease to zero stress value.

Figure 4 shows bar-charts of σ, E, u' and u versus POSS concentration. Results from the control group (0% (w/w)) are included for the purpose of comparison. One-way ANOVA of each of the mechanical parameter, σ, u' and u, shows *P*-values $<$ 0.01. This indicates that there is strong

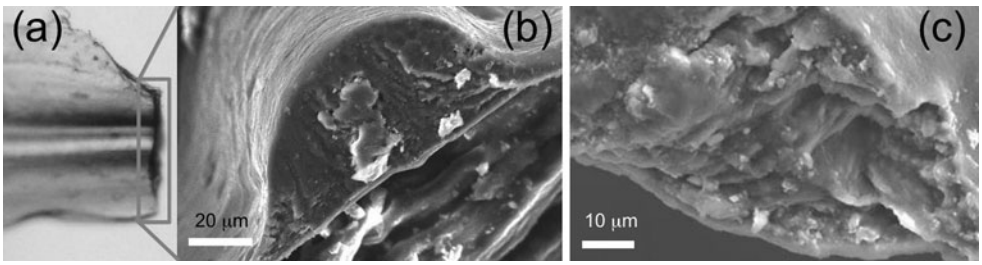

Fig. 3 POSS-chitosan microfibre as seen under a light microscope (**a**). Field-emission scanning electron microscopy reveals the **b** triangular-like cross-section (prepared using a razor), and **c** fractured ends (from tensile testing)

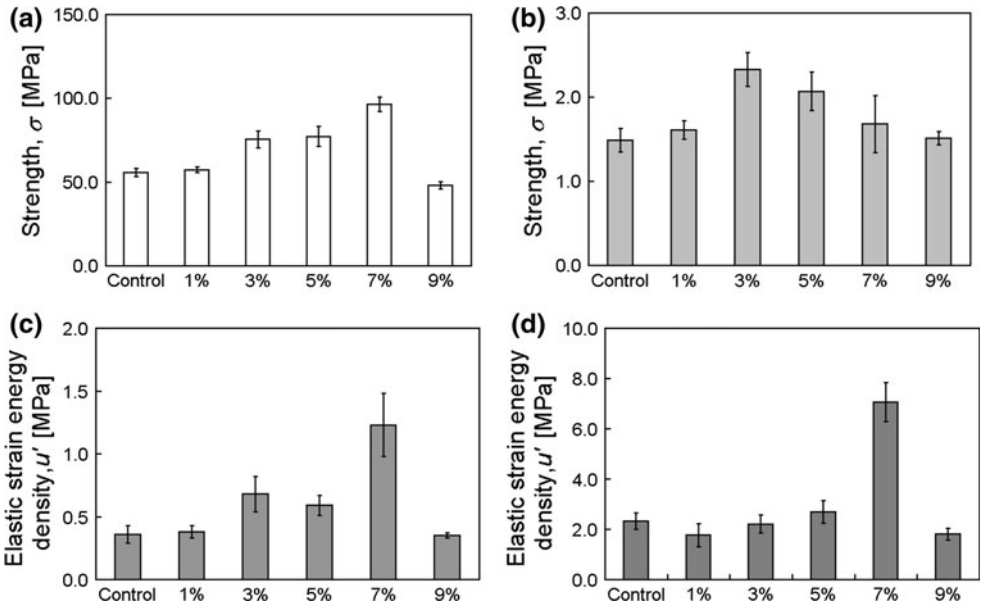

Fig. 4 Bar charts showing **a** strength, σ, **b** stiffness. E, **c** elastic strain energy density, u', and **d** fracture strain energy density, u, versus POSS concentration (% w/w). Vertical bars indicate standard error. Results from the control group (0% (w/w)) are shown here for the purpose of comparison

evidence to conclude that not all the means (i.e. associated with the different POSS concentration) of the respective mechanical parameter are equal when the level of significance is set at 0.01. Tukey's test yields five sets of confidence intervals (CIs) for the respective mechanical parameter. Pair-wise multiple comparison of the CIs for those that exclude zero yields the following results. No appreciable difference is observed in the magnitudes of σ between the 1% (w/w) and the control groups (the latter yields $\sigma = 5.85 \pm 2.45$ MPa). From 3 to 7% (w/w), it is observed that σ increases with increasing POSS concentration, attaining a maximum value of 99.46 ± 4.33 MPa at 7% (w/w), which is approximately 1.73 times larger than the control. Beyond 7% (w/w), the magnitude of σ decreases; in particular, it is observed that the magnitude of σ at 9% (w/w) yields no significant difference with the control group. Similar results have been achieved with u' and u. The 7% (w/w) group yields $u' = 1.23 \pm 0.25$ MPa and $u = 7.06 \pm 0.78$ MPa. (c.f. the control group, i.e. $u' = 0.36 \pm 0.07$ MPa and $u = 2.33 \pm 0.32$ MPa). Thus u' and u from the 7% (w/w) group are approximately 3.42 and 3.03 times larger than the control group.

In the case for E, one-way ANOVA shows P-value $= 0.043$. This suggests that not all the means of E (i.e. associated with the different POSS concentration) are equal when the level of significance is set at 0.01. However, pair-wise comparison of the CIs from all groups using Tukey's test (i.e. at family error rate $= 0.01$) reveals that the CIs include the zero value. This implies that all groups yield no significant difference in E. Owing to the discrepancy between the results from ANOVA and the Tukey test, and considering that the P-value $= 0.043$ is close to 0.01, we recommend interpreting the ANOVA results conservatively.

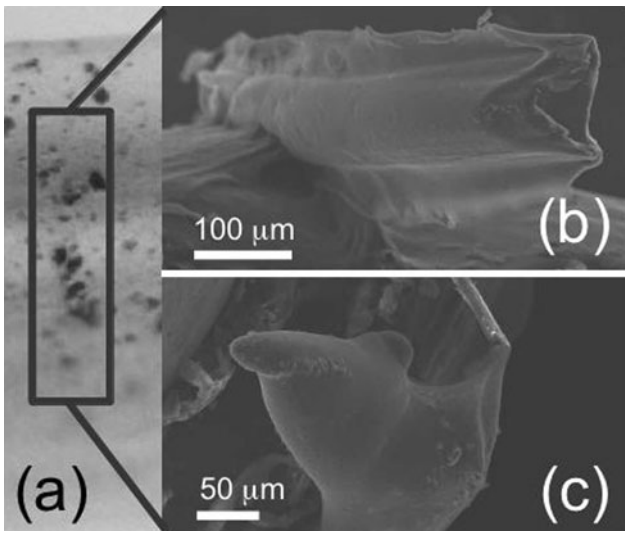

Fig. 5 Morphological modifications to a POSS-Chitosan microfibre (**a**) by the simulated body fluid. Field-emission scanning electron microscopy reveals grossly distorted morphology of microfibres, accompanied by the appearance of highly irregular stumps (**b**) and (**c**)

3.3 Bioactivity

After immersing in the SBF over a period of 4 days, the mass of the microfibres increased by about 1.36 times on average. Under an optical microscope, the surfaces of the fibre appear to have been peeled; numerous 'pin-like' holes are also observed. Analysis of the SEM images reveals grossly distorted morphology of microfibres, which is accompanied by the appearance of highly irregular stumps (out-growths) protruding outward (Fig. 5b) or running along (Fig. 5c) the microfibres. These stumps may be evidence of the deposition of new materials.

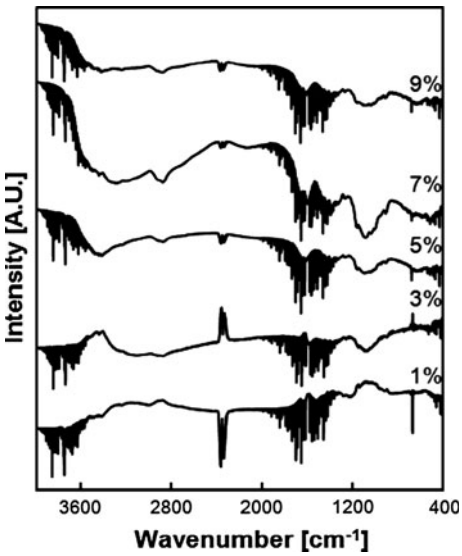

Fig. 6 Fourier transform infra-red spectra for different concentrations (w/w) of POSS reinforcing chitosan-based microfibre

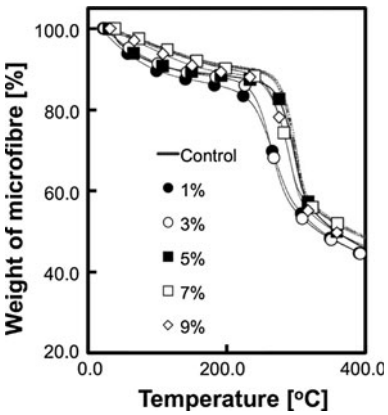

Fig. 7 Graph of weight of microfibre (%) versus temperature (Celsius) for 1, 3, 5, 7 and 9% (w/w) of POSS reinforcing chitosan-based microfibre (thick line) and the control group (0% w/w; thin line)

3.4 Compositional characteristics

The FT-IR spectra for different concentrations of PC microfibres present the characteristic absorption bands of chitosan, chitin and POSS (Fig. 6). The basic characteristics of chitosan, i.e. H-bonds (3450–3600 cm^{-1}), C–O stretching vibrations (990–1060 cm^{-1}) and amine N–H bending vibrations (1600–1450 cm^{-1}), are clearly observed in all samples. The presence of peak at ca. 1650 cm^{-1}, corresponding to amide C=O stretching, the main characteristic peak of chitin, suggests that chitosan is a partially deacetylated product [35]. The band at 1120 cm^{-1}, arising from the stretching (vibration) of Si–O–Si, has been observed [36]. This indicates that POSS has been blended in the chitosan matrix. No significant increase is observed in the peak intensity at 1120 cm^{-1} with increasing POSS concentrations and this indicates that POSS has been fairly uniformly dispersed in the chitosan matrix. All samples show the presence of peak at ca. 2350 cm^{-1} which are due to the ambient carbon dioxide [37]. There is an absence of peaks associated with new bonds arising from co-polymerisation of POSS and the chitosan biopolymer.

3.5 Thermal stability

Thermogravimetric (TG) measurements in nitrogen atmosphere indicate that chitosan and PC microfibres exhibit quite similar TG trends (Fig. 7). An initial weight loss from ambient temperature to 240°C corresponds to the evaporation of adsorbed water. The predominant stage of thermal degradation appears in the range of 240–350°C and it may be attributed to the degradation of saccharide structure of the chitosan composite. TGA shows that the PC microfibers is thermally stable up 240°C. This finding agrees with that reported by Knaul et al. who revealed that the chitosan backbone did not experience thermal degradation under normal conditions at temperatures below 250°C [30]. The residues of chitosan and PC microfibres after heating at 500°C are around 40 wt%. (Consequently, PC microfibre may be useful for biomedical applications such as drug eluting devices and bioscaffolds for tissue implants, because the degradation temperature is above human body temperature of 37°C.)

4 Discussion

4.1 Structure–property relationship

An important consideration in the characteristics of the PC microfibres investigated here is the role of POSS for enhancing σ, u' and u at low POSS concentration and the diminishing influence of POSS at higher POSS concentration. Before presenting our arguments to support this observation, namely by addressing the structure–property relationship of the PC microfibre, we note the following points on the molecular scale:

(1) The 7 phenyl and 1 ethylamine organic groups of the co-monomer aminopropylphenyl POSS are covalently bonded to the respective Si atoms. The ethylamine groups are reactive and can undergo bulk polymerizations [38]. Alternatively, it has been pointed out that interaction among the POSS co-monomers can arise from van der Waals (VDW) forces between the groups on adjacent co-monomers, producing clusters of POSS molecules around a backbone axis [28]. In these respects, it is to be expected that the interaction increases

with the number of cages in the POSS cluster, eventually leading to energetically stable precipitates that sterically inhibit further reaction with another POSS co-monomer.

(2) At the PC interface, the phenyl groups contribute to solubilizing the inorganic core and, to a certain extent, facilitating the interaction of the POSS precipitates with the surrounding chitosan biopolymers by direct noncovalent bonding involving the hydrogen bonds with the respective NH_2 and OH groups on the chitosan molecule [39, 40]. However, how the chitosan biopolymer conformation changes to adapt to the POSS is not clear.

(3) The chitosan matrix is held together by interactions between the C and O atoms on the respective molecules, giving rise to three possible pairs, namely O–O, O–C and C–C in the order of increasing bond energy [40].

The ability of POSS to provide reinforcement may be explained by the stress transfer theory [41]. When the microfibre is loaded, the chitosan matrix deforms and slides over the surface of the POSS precipitates. In turn, frictional shear stress (τ) is generated at the PC interface. The action of τ on the POSS precipitate causes the precipitate to deform and generates stresses. The magnitude of τ depends on the extent of contact between the chitosan matrix and POSS. As the load increases, when the stress in the POSS precipitate exceeds the strength of POSS, cracks appear in the precipitate as the interaction between POSS molecules are disrupted (see # 1). As the cracks grow, the area of high stresses ahead of each crack propagates to the PC interface. Non-covalent interactions at the PC interface (see # 2) actually strengthen the microfibre by deflecting the crack growth when the crack tip reaches the PC interface. Consequently, a crack trap or crack stopper is created as the crack is unable to cross this interface and propagate to the other precipitates rapidly. However, when the precipitate ruptures into two, the chitosan matrix surrounding the ruptured precipitate will have to accommodate higher stress; when this stress reaches the strength of chitosan, cracks appear in the matrix (see #3). As cracks propagate and merge with others to grow in size eventually the microfibre ruptures into two.

4.2 Effects of POSS concentration

Application of the rule of mixtures model for particulate reinforcement to evaluating the relationship between POSS concentration and σ [42] yields

$$\sigma = \sigma_P V_P + \sigma_C V_C \quad (1)$$

where the relative concentrations of POSS and chitosan are represented by the volume fractions, i.e. V_P and V_C, respectively ($V_P + V_C = 1$); σ_P and σ_C represent the in situ strengths of POSS and chitosan, respectively. Given that the densities of POSS is 1.20 g/cm^3 and that of chitosan is 0.3 g/cm^3, it is easy to see that 1, 3, 5, 7 and 9% (w/w) POSS correspond to $V_P = 0.003$, 0.008, 0.013, 0.018 and 0.024, respectively. By considering V_P from 0 to 0.018, linear regression analysis of σ versus V_P reveals that σ increases at a rate of 2.22 ± 0.29 GPa for every unit increase in V_P ($F = 60.51$, $P < 0.01$, $R^2 = 69.9\%$). Consequently, this model (Eq. 1) predicts that $\sigma_P = 2.28 \pm 0.29$ GPa. This model shows that the critical volume fraction, V_{min} [42], beyond which the chitosan matrix will not be able to support the entire load when the POSS precipitates fragment is 0.018 (7% (w/w)). Hydroxyapatite (HA, $Ca_{10}(PO_4)_6(OH)_2$), a nontoxic and noninflammatory mineral content comprising 43% of overall bone weight [43], reinforcing chitosan yields a much lower in situ strength of 0.13 ± 0.02 GPa [3]. Clearly, at higher POSS concentration the additional POSS that coalesces among the chitosan biopolymers acts as a filler with little or low adhesion to the chitosan matrix (Sect. 4.1 [44]). Consequently, little or no stress is transferred to the precipitates (Sect. 4.1); at sufficiently high load, the precipitates detach easily among themselves. Thus, the additional POSS is not only unable to support the microfibre but also compromise σ.

An energy analysis of work done on the microfibre to cause fracture suggests a possible model for describing how the work of fracture, G, is influenced by V_f, σ_P, the diameter of the POSS particulate (D) and the shear stress at the PC interface (τ), according to [45]. Scaling G, i.e. dividing by the length of the specimen (L), yields a parameter associated to u. Correspondingly, u is related to V_f, σ_P, D, τ and L as follows,

$$u \sim \frac{\sigma_P^2 V_P D}{24 \tau L} \quad (2)$$

The bonds within POSS absorb energy and stretch (Sect. 4.1) as the microfibre deforms. Clearly the extent of this elastic disturbance to the fine structure of deep-lying precipitates is regulated by the concentration of POSS. Thus, the deeper is the disturbance into the microfibre the larger is the magnitude of u. Similarly, by considering V_P from 0 to 0.018 (corresponding to the peak value of u), linear regression analysis of u versus V_P (assuming that σ_P, D and τ are constants) reveals that u increases at a rate of 240.6 ± 48.0 MPa for every unit increase in V_P ($F = 25.13$, $P < 0.01$, $R^2 = 49.1\%$). Accordingly, the P value corresponding to the y-intercept is observed to be <0.01.

Broadly, E is a measure of the stress to double the length of the microfibre before yielding occurs. When the microfibre is loaded initially, local deformation leads to straightening of the bent, kinked and convoluted bonds

between the monomers of the flexible chitosan biopolymer (Sect. 4.1); none of this kind happens in the siliceous nucleus of the POSS molecule where the load is required to pull directly on the interatomic bonds. According to the ANOVA test, since no significant difference in E is observed with respect to POSS concentration (Sect. 3.2) this suggests that the molecular flexibility of the biopolymer is not significantly impeded by the interactions with the neighbouring POSS precipitates (Sect. 4.1).

4.3 Mechanical reliability

Defects arising from within the POSS clusters, or even local non-uniform dispersion of POSS particulates within the microfibre, can act as stress intensifiers and initiate fractures when they induce sufficiently large stresses to mechanically break chemical bonds (Sect. 4.1). From Weibull's empirical law, the cumulative distribution function (C) of σ [46] for determining failure due to flaws is given by

$$C(\sigma) = 1 - \exp(-[\sigma/\sigma_0]^m), \quad (3)$$

which quantifies the probability of a microfibre surviving at a stress lower than or equal to σ. Here, m and σ_0 represent the Weibull modulus and the characteristic strength, respectively; m parameterizes the variability of σ, e.g. low m values correspond to high variability and vice versa while σ_0 is the stress value at which $\sim$63% of the fibres have fractured. To estimate the values of m and σ_0 for the different treatment groups, first, the median rank position (M_R) for each experimentally derived value of σ was evaluated. By ranking the σ data in ascending order of magnitude this yields the corresponding estimates of M_R (=$[i - 0.3]/[n + 0.4]$) where n represents the size of the group and i is the position of the corresponding σ. For each group straight lines were fitted to the Weibull plot of $\log(\log(1/(1 - M_R(\sigma))))$ versus $\log(\sigma)$ (according to Eq. 3) to yield the corresponding m and σ_0 values (Table 1); here we note that the value of m is equal to the slope of the regressed line while the value of σ_0 was found by equating $-m\log(\sigma_0)$ to the y-intercept (Fig. 8 inset). For plots of the cumulative distribution function versus σ for microfibres of different POSS concentrations see Fig. 8. Interestingly, this simple analysis predicts that the microfibres from the group with 5% (w/w) POSS exhibit the smallest strength variability of m while those from the 1% POSS group exhibit the largest strength variability. However, the Weibull model predicts that increasing POSS concentration yields a corresponding increase in the magnitude of σ_0 (from 0 to 7% (w/w)) followed by a decrease at 9% (w/w), consistent with the trend obtained for σ (Sect. 3.2).

Table 1 Analysis of the Weibull modulus, m, and the characteristic strength, σ_0, of chitosan-based microfibres reinforced by 1, 3, 5, 7 and 9% (w/w) POSS

Treatment	m	σ_0 (MPa)
Control	8.77	58.83
1%	14.87	59.15
3%	5.97	81.14
5%	5.76	83.11
7%	9.17	101.38
9%	10.00	50.16

Results from the control group are shown for the purpose of comparison

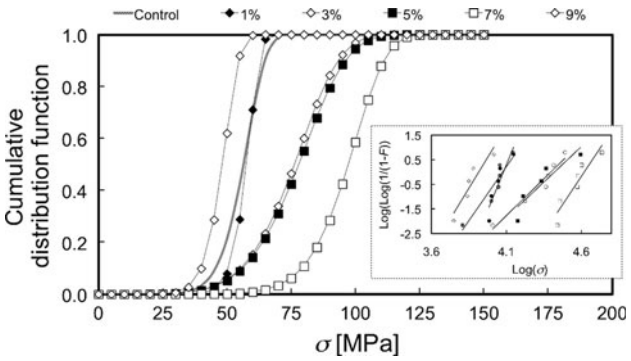

Fig. 8 Plot of Weibull's cumulative distribution function versus σ. Inset shows a graph of $\log(\log(1/(1 - M_R)))$ versus $\log(\sigma)$ to assess the variability of σ for different POSS concentrations; here M_R represents the median rank position as a function of σ order number. The result from the control group (0% (w/w)) is shown here for the purpose of comparison

4.4 Bioactivity

The mass of the microfibres increases after 3–4 days of immersing in simulated body fluid. Further examination of the surface morphology reveals features such as stumps. Since Ca^{2+} and HPO_4^{2-} ions are present in the SBF (apart from Na^+, K^+, Mg^{2+}, Cl^-, HCO_3^{3-}, and SO_4^{2-}), it is likely that the stumps are apatites deposits, ($Ca_{10}(PO_4)_6(OH)_2$). The mechanism of apatite nucleation may be similar to those formed on the surfaces of bioactive glasses and glass–ceramics [47]. In this case, the mechanism addresses the exchange of the amine with an OH on the POSS molecule, resulting in a silanol group, which is responsible for regulating apatite nucleation [31]. It is also likely that chitosan is involved in apatite nucleation [48]. Owing to the abundance of free amine groups, chitosan is reactive [49], i.e. in this case it undergoes phosphorylation readily [50] with the SBF. We note that although chitosan is not dissolvable in water under neutral pH, it is easily swollen in aqueous solutions; the POSS-Chitosan composite has been known to swell as much as 1.5 times [51].

Consequently, this could also contribute to the change in the shape and mass of the microfibre.

5 Conclusions

A study has been carried out to synthesize and characterize PC microfibres. A wet-spinning approach was used to fabricate the microfibres. Tensile testing reveals that POSS influences σ, u' and u. (However, POSS has no effect on E.) In particular, it is observed that σ, u' and u increase with increasing POSS concentration from 0 to 7% (w/w). However, on further increase in the POSS concentration, it is observed that σ, u' and u decrease. FESEM reveals that the PC microfibres fail by brittle fracture. TGA reveals that high degradation temperature of the PC microfibre (well above human body temperature of 37°C). Bioactivity test using SBF reveals appreciable degradation in the PC microfibres at day 4. The tailorable mechanical properties, in addition to bioactivity and thermal stability suggest that the PC microfibres may be useful for biomedical applications such as drug eluting devices and bioscaffolds for tissue implants.

Acknowledgments This project was funded by grants from the Singapore Ministry of Education (AcRF 34/06) and Collier Charitable Trust (CF09/3638).

References

1. Bhattarai N, Edmondson D, Veiseh O, Matsen FA, Zhang M. Electrospun chitosan-based nanofibers and their cellular compatibility. Biomaterials. 2005;26:6176–84.
2. Geng X, Kwon O-H, Jang J. Electrospinning of chitosan dissolved in concentrated acetic acid solution. Biomaterials. 2005; 26:5427–32.
3. Xie JZ, Hein S, Wang K, Liao K, Goh KL. Influence of hydroxyapatite crystallization temperature and concentration on stress transfer in wet-spun nanohydroxyapatitechitosan composite fibres. Biomed Mater. 2008;3:025014.
4. Wang JZ, Huang XB, Xiao J, Li N, Yu WT, Wang W, Xie WY, Ma XJ, Teng YL. Spray-spinning: a novel method for making alginate chitosan fibrous scaffold. J Mater Sci: Mater Med. 2010;21:497–506.
5. Meng W, Xing ZC, Jung KH, Kim SY, Yuan J, Kang IK, Yoon SC, Shin HI. Synthesis of gelatin-containing PHBV nanofiber mats for biomedical application. J Mater Sci: Mater Med. 2008;19:2799–807.
6. He QR, Zhang TY, Yang YM, Ding F. In vitro biocompatibility of chitosan-based materials to primary culture of hippocampal neurons. J Mater Sci: Mater Med. 2009;20:1457–66.
7. Cao Y, Rodriguez A, Vacanti M, Ibarra C, Arevalo C, Vacanti CA. Comparative study of the use of poly(glycolic acid), calcium alginate and pluronics in the engineering of autologous porcine cartilage. J Biomater Sci Polym Ed. 1998;9:475–87.
8. Abe M, Takahashi M, Tokura S, Tamura H, Nagano A. Cartilage–scaffold composites produced by bioresorbable β-chitin sponge with cultured rabbit chondrocytes. Tissue Eng. 2004;10:585–94.
9. Ragetly GR, Griffon DJ, Lee H-B, Chung YS. Effect of collagen II coating on mesenchymal stem cell adhesion on chitosan and on reacetylated chitosan fibrous scaffolds. J Mater Sci: Mater Med. 2010;21:2479–90.
10. Hirano S. Wet-spinning and applications of functional fibers based on chitin and chitosan. Macromol Symp. 2001;168:21–30.
11. Yang YM, Hu W, Wang XD, Gu XS. The controlling biodegradation of chitosan fibers by N-acetylation in vitro and in vivo. J Mater Sci: Mater Med. 2007;18:2117–21.
12. Enescu D, Olteanu CE. Functionalized chitosan and its use in pharmaceutical, biomedical, and biotechnological research. Chem Eng Commun. 2008;195:1269–91.
13. Langer R, Tirrell DA. Designing materials for biology and medicine. Nature. 2004;428:487–92.
14. Agarwal D, Matthew HWT. Branched chitosans: effects of branching parameters on rheological and mechanical properties. J Biomed Mater Res A. 2007;82:201–12.
15. Silver FH, Bradica G, Tria AJ. Elastic energy storage in human articular cartilage: estimation of the elastic modulus for type II collagen and changes associated with osteoarthritis. Matrix Biol. 2002;21:129–37.
16. Moretti M, Wendt D, Schaefer D, Jakob M, Hunziker EB, Heberera M, Martin I. Structural characterization and reliable biomechanical assessment of integrative cartilage repair. J Biomech. 2005;38:1846–54.
17. Rotter N, Bonassar LJ, Tobias G, Lebl M, Roy AK, Vacanti CA. Age dependence of biochemical and biomechanical properties of tissue-engineered human septal cartilage. Biomaterials. 2002;23: 3087–94.
18. Zioupos P, Currey JD. Changes in the stiffness, strength, and toughness of human cortical bone with age. Bone. 1998;22:57–66.
19. Kayacan R. The effect of staining on the monotonic tensile mechanical properties of human cortical bone. J Anat. 2007;211: 654–61.
20. Kannan RY, Salacinski HJ, Butler PE, Seifalian AM, Butler PE. Polyhedral oligomeric silsesquioxane nanocomposites: the next generation material for biomedical applications. Acc Chem Res. 2005;38:879–84.
21. Cordes DB, Lickiss PD, Ratabou F. Recent developments in the chemistry of cubic polyhedral oligosilsesquioxanes. Chem Rev. 2010;110:2081–173.
22. Flodin JT, Lichtenhan JD, Schwab JJ, An Y-Z, Fu X, Kemp Z. Biomimetic materials comprising polyhedral oligomeric silsesquioxanes. Patent Application Publication. July 9 2009; US2009/0176006 A1.
23. Bleha M, Tishchenko G, Pientka Z, Brus J. Effect of POSS functionality on morphology of thin hybrid chitosan films. Des Monomers Polym. 2004;7:25–43.
24. Yoshitake H, Koiso E, Horie H, Yoshimura H. Polyamine-functionalized mesoporous silicas: preparation, structural analysis and oxyanion adsorption. Micropor Mesopor Mater. 2005;85:183–94.
25. Syomin D, Kim J, Koel BE, Ellison GB. Identification of absorbed phenyl (C6H5) groups on metal surfaces: electron-induced dissociation of benzene on Au(111). J Phys Chem. 2001;105:8387–94.
26. Waddon AJ, Couhlin EB. Crystal structure of polyhedral oligomeric silsequioxane (POSS) nano-materials: a study by X-ray diffraction and electron microscopy. Chem Mater. 2003;15: 4555–61.
27. Dalton AB, Collins S, Munoz E, Razal JM, Ebron VH, Ferraris JP, Coleman JN, Kim BG, Baughman RH. Super-tough carbon-nanotube fibres. Nature. 2003;423:703.
28. Anderson SE, Baker ES, Mitchell C, Haddad TS, Bowers MT. Structure of hybrid polyhedral oligomeric silsesquioxane propyl methacrylate oligomers using ion mobility mass spectrometry and molecular mechanics. Chem Mater. 2005;17:2537–45.

29. Zheng L, Hong S, Cardoen G, Burgaz E, Gido SP, Coughlin EB. Polymer nanocomposites through controlled self-assembly of cubic silsesquioxane scaffolds. Macromolecules. 2004;37: 8606–11.
30. Knaul J, Hooper M, Chanyi C, Creber KAM. Improvements in the drying process for wet-spun chitosan fibers. J Appl Polym Sci. 1998;69:1435–44.
31. Cho S-B, Nakanishi K, Kokubo T, Soga N, Ohtsuki C, Nakamura T. Apatite formation on silica gel in simulated body fluid: its dependence on structures of silica gels prepared in different media. J Biomed Mater Res App1 Biomater 1996;33:145–51.
32. Oyane A, Kim H-M, Furuya T, Kokubo T, Miyazaki T, Nakamura T. Preparation and assessment of revised simulated body fluids. J Biomed Mater Res. 2003;65A:188–95.
33. Goh KL, Holmes DF, Lu H-Y, Richardson S, Kadler KE, Purslow PP, Wess TJ. Ageing changes in the tensile properties of tendons: influence of collagen fibril volume fraction. J Biomech Eng. 2008;130:021011–2.
34. Goh KL, Chen Y, Chou SM, Listrat A, Bechet D, Wess TJ. Effects of frozen storage temperature on the elasticity of tendons from a small murine model. Animal. 2010;4:1613–7.
35. Sionkowska A, Wisniewski M, Skopinska J, Kennedy CJ, Wess TJ. Molecular interactions in collagen and chitosan blends. Biomaterials. 2004;25:795–801.
36. Zhou Z, Cui L, Zhang Y, Zhang Y, Yin N. Preparation and properties of POSS grafted polypropylene by reactive blending. Eur Polym J. 2008;44:3057–66.
37. Kim SH, Kim JW, Im JS, Kim YH, Lee YS. A comparative study on properties of multi-walled carbon nanotubes (MWCNTs) modified with acids and oxyfluorination. J Fluorine Chem. 2007;128:60–4.
38. Haddad TS, Viers BD, Phillips SH. Polyhedral oligomeric silsesquioxane (POSS)-styrene macromers. J Inorg Organomet Polym. 2002;11:155–64.
39. Strachota A, Tishchenko G, Matejka L, Bleha M. Chitosan–oligo(silsesquioxane) blend membranes: preparation, morphology, and diffusion permeability. J Inorg Organomet Polym. 2002; 11:165–82.
40. Tishchenko G, Bleha M. Diffusion permeability of hybrid chitosan/polyhedral oligomeric silsesquioxanes (POSSTM) membranes to amino acids. J Membr Sci. 2005;248:45–51.
41. Goh KL, Aspden RM, Hukins DWL. Review: finite element analysis of stress transfer in short-fibre composite materials. Compos Sci Technol. 2004;64:1091–100.
42. Kelly A, Macmillan NH. Strong solids. 3rd ed. Oxford: Oxford University Press; 1986.
43. Di Martino A, Sittinger M, Risbud MV. Chitosan: a versatile biopolymer for orthopaedic tissue-engineering. Biomaterials. 2005;26:5983–90.
44. Zhao Y, Schiraldi DA. Thermal and mechanical properties of polyhedral oligomeric silsesquioxane (POSS)/polycarbonate composites. Polymer. 2005;46:11640–7.
45. Piggott MR. Load-bearing fibre composites. Oxford: Pergamon Press; 1987.
46. Weibull W. A statistical distribution function of wide applicability. J Appl Mech. 1951;18:293–7.
47. Kokubo T, Takadama H. How useful is SBF in predicting in vivo bone bioactivity? Biomaterials. 2006;27:2907–15.
48. Tuzlakoglu K, Reis RL. Formation of bone-like apatite layer on chitosan fiber mesh scaffolds by a biomimetic spraying process. J Mater Sci: Mater Med. 2007;18:1279–86.
49. Yi HM, Wu LQ, Bentley WE, Ghodssi R, Rubloff GW, Culver JN, Payne GF. Biofabrication with chitosan. Biomacromolecules. 2005;6:2881–94.
50. Wan Y, Creber KAM, Peppley B, Bui VT. Synthesis, characterization and ionic conductive properties of phosphorylated chitosan membranes. Macromol Chem Phys. 2003;204:850–8.
51. Xu D, Loo L, Wang K. Pervaporation performance of novel chitosan-POSS hybrid membranes: effects of poss and operating conditions. J Polym Sci B: Polym Phys. 2010;48:2185–92.